[10] H. J. Butterweck, "Orthogonal Kirchhoff modes—A new tool of network analysis," *IEEE Trans. Circuit Theory*, vol. CT-19, pp. 307–312, July 1972.
[11] E. Stiefel, *Introduction to the Numerical Mathematics* (in German). Stuttgart, Germany: Teubner, 1965, p. 21.
[12] S. W. Director, "*LU* factorization in network sensitivity computation," *IEEE Trans. Circuit Theory* (Corresp.), vol. 18, pp. 184–185, Jan. 1971.
[13] V. Strassen, "Gaussian elimination is not optimal," *Numer. Math.*, vol. 13, pp. 354–356, 1969.
[14] J. te Winkel, "Drift transistor, simplified electrical characterization," *Electron. Radio Eng.*, pp. 2–10, Aug. 1959.
[15] H. F. Cooke, "Microwave transistors: Theory and design," *Proc. IEEE (Special Issue on Microwave Semiconductors)*, vol. 59, pp. 1163–1181, Aug. 1971.
[16] T. Downs, "An approach to the computation of network sensitivities," *Marconi Rev.*, 3rd qr., pp. 205–212, 1972.
[17] J. W. Bandler and R. E. Seviora, "Current trends in network optimization," *IEEE Trans. Microwave Theory Tech. (1970 Symposium Issue)*, vol. MTT-18, pp. 1159–1170, Dec. 1970.
[18] ——, "Wave sensitivities of networks," *IEEE Trans. Microwave Theory Tech.*, vol. MTT-20, pp. 138–148, Feb. 1972.
[19] ——, "Direct method for evaluating scattering matrix sensitivities," *Electron. Lett.*, pp. 773–774, 1970.
[20] V. A. Monaco and P. Tiberio, "On linear network scattering matrix sensitivity," *Alta Freq.*, vol. 39, pp. 193–195, Feb. 1970.
[21] G. Iuculano, V. A. Monaco, and P. Tiberio, "Network sensitivities in terms of scattering parameters," *Electron. Lett.*, pp. 53–55, Jan. 1971.
[22] K. Hartmann and M. J. O. Strutt, "Changes of the four noise parameters due to general changes of linear two-port circuits," *IEEE Trans. Electron Devices*, vol. ED-20, pp. 874–877, Oct. 1973.
[23] K. Hartmann, "The small signal and noise behavior of microwave bipolar transistors up to 12 GHz," in *Proc. European Microwave Conf.* (Brussels, Belgium, Sept. 4–7, 1973).
[24] K. Hartmann, W. Kotyczka, and M. J. O. Strutt, "Computerized determination of electrical network noise due to correlated and uncorrelated noise sources," *IEEE Trans. Circuit Theory* (Short Paper), vol. CT-20, pp. 321–322, May 1973.
[25] B. Schneider and M. J. O. Strutt, "Theory and experiments on shot noise in silicon *P-N* junction diodes and transistors," *Proc. IRE*, vol. 47, pp. 546–554, Apr. 1959.
[26] ——, "Shot and thermal noise in germanium and silicon transistors at high-level current injections," *Proc. IRE*, vol. 48, pp. 1731–1739, Oct. 1960.
[27] K. Hartmann, "Computer simulation of linear noisy two-port circuits with special consideration of the bipolar transistor up to 12 GHz." (in German), Ph.D. dissertation 5118, Swiss Federal Institute of Technology, Zurich, Switzerland, 1973.

A Theoretical Study of the High-Frequency Performance of a Schottky-Barrier Field-Effect Transistor Fabricated on a High-Resistivity Substrate

GARY D. ALLEY, MEMBER, IEEE, AND HARRY E. TALLEY, SENIOR MEMBER, IEEE

Abstract—**The short-circuit admittance parameters for a silicon Schottky-barrier field-effect transistor (SBFET) fabricated on a high-resistivity substrate are calculated from first principles ignoring the effects of minority carriers. The calculations show the maximum frequency of oscillation for a device with a 1-μm gate to be 17.9 GHz, neglecting the parasitics associated with the contact metallizations, and 14.7 GHz when the parasitics are included.**

In order to describe the dynamic behavior of the device, the static properties must first be obtained. The simultaneous solution of Poisson's equation and the continuity equation, both in two dimensions, gives the static charge and potential distribution in the device. The effects of a field-dependent mobility are included in the continuity equation. Using the results of static two-dimensional solutions, a one-dimensional device model is developed that permits the dynamic device behavior to be described by a one-dimensional linear ordinary differential equation. By solving this equation under appropriate boundary conditions, the device y parameters are found as functions of frequency. Calculated results are shown to be in good agreement with published experimental data.

Manuscript received July 3, 1973; revised November 9, 1973. This work is based on a paper presented at the 1972 IEEE International Electron Device Meeting, Washington, D. C., Dec. 4–6, 1972.

G. D. Alley was with the Department of Electrical Engineering, University of Kansas, Lawrence, Kans. He is now with Bell Laboratories, North Andover, Mass.

H. E. Talley is with the Department of Electrical Engineering, University of Kansas, Lawrence, Kans.

I. Introduction

THE DEMONSTRATED high-frequency capabilities of field-effect transistors [1] indicate that they will have important applications in microwave systems. In this paper we present a method for calculating the y parameters as a function of frequency for a silicon Schottky-barrier field-effect transistor (SBFET) [2]. The results of these calculations are valid up to and beyond the maximum frequency of oscillation for a given device, so that the method may be used to optimize the high-frequency response of an SBFET. The theoretical calculations presented are compared with experimental data published in the literature and are shown to be in good agreement.

In order to obtain the desired y parameters, we first solve simultaneously the continuity equation and Poisson's equation, both in two dimensions, in order to find the

static charge and potential distribution in a two-dimensional model of the device. Using the results of these static solutions, a one-dimensional model is completely specified that permits the dynamic device behavior to be described by a one-dimensional linear ordinary differential equation. It is important to note that there are no arbitrary constants in this analysis. By solving this equation under appropriate boundary conditions, the device y parameters are found as functions of frequency. In both the static and dynamic cases we have explicitly included the dependence of the electron mobility on the electric field existing in the device.

II. Static Description of an SBFET

Before the small-signal behavior of an SBFET can be investigated we must find the static charge and potential distribution in the device. A cross section of the device to be studied showing pertinent dimensions and impurity concentrations is shown in Fig. 1. We assume the gate length (perpendicular to the plane of Fig. 1) to be 400 μm.

The two-dimensional continuity equations for holes and electrons together with the two-dimensional Poisson equation govern the behavior of the two-dimensional model of the device [3]. Because the SBFET is basically a majority carrier device, we have chosen to ignore minority carriers [4].

We formulate the problem in terms of the electrostatic (Ψ) and the quasi-Fermi level for electrons (ϕ). The resulting equations are

$$\bar{J} = -q\mu n \frac{\partial \phi}{\partial x}\bar{\imath} - q\mu n \frac{\partial \phi}{\partial y}\bar{\jmath} = \bar{J}_x\bar{\imath} + J_y\bar{\jmath} \tag{1}$$

$$-\frac{\partial n}{\partial t} = -g + r - \frac{1}{q}\frac{\partial J_x}{\partial x} - \frac{1}{q}\frac{\partial J_y}{\partial y} \tag{2}$$

$$\frac{\partial^2 \psi}{\partial x^2} + \frac{\partial^2 \psi}{\partial y^2} = \frac{-q}{\epsilon}(N_d - n) \tag{3}$$

$$n = n_i e^{\gamma(\psi - \phi)}, \qquad \gamma = \frac{q}{kT}. \tag{4}$$

Because of the high fields that are expected to occur in the channel, the field-dependent mobility is included using the empirical relation due to Jaggi [5]:

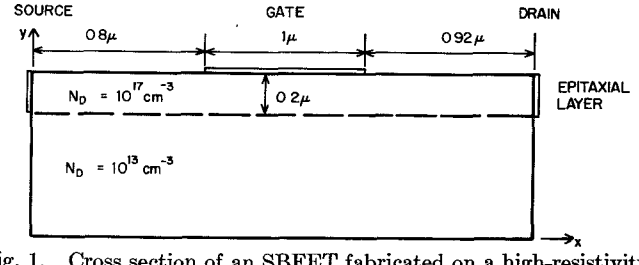

Fig. 1. Cross section of an SBFET fabricated on a high-resistivity substrate showing the dimensions and impurity concentrations.

$$\mu = 2\mu_0 \Big/ \left\{1 + \left[1 + \left(\frac{2\mu_0 E}{v_s}\right)^2\right]^{1/2}\right\} \tag{5}$$

in which μ_0 is the low field mobility, v_s the electron scattering limited velocity, and E the magnitude of the electric field. The mobility is taken to be a scalar depending only upon the magnitude of the electric field.

The set of equations (1)–(5) was solved subject to appropriate boundary conditions using finite difference methods and under-relaxation. Although the formulation of the problem is different, the device characteristics obtained using the static two-dimensional calculations were quite similar to those reported by Reiser [4], [6], Kennedy and O'Brien [3], and Kim and Yang [7]. In the interests of brevity these results will not be shown. We do, however, make extensive use of them in deriving the parameters of the one-dimensional ac model.

III. Dynamic Description of an SBFET

A. Equations Governing the One-Dimensional AC Model

In principle we could assume harmonic variation of the appropriate variables and solve the set of equations (1)–(5) to obtain the time-dependent electrostatic potential and quasi-Fermi level and from these the ac currents and voltages. These voltages and currents could then be used to obtain the y parameters. The resulting ac equations would be linear and, therefore, straightforward to solve. Even with a sparse grid, however, the calculation time would be very great, particularly with the realization that we would need to calculate the complex y parameters for 20 or 30 frequencies.

For this reason, we have chosen to try to develop a one-dimensional model of the ac behavior of the SBFET. In this section we will develop the equations describing the model and in Section III-B the model parameters will be deduced. The parameters of the one-dimensional model will be derived by averaging certain quantities obtained from the two-dimensional static solution.

The ac model is based on the one-dimensional continuity equation and, as in previous models [9]–[11], a knowledge of the channel to gate capacitance as a function of the dimension parallel to the gate. The one-dimensional current flow equation is given in (6) in terms of separate drift and diffusion terms. The one-dimensional continuity equation is given in (7), where we have ignored the generation and recombination terms

$$I = -Q\mu \frac{dV}{dx} + \gamma\mu \frac{dQ}{dx} \tag{6}$$

$$\frac{dI}{dx} = -\frac{dQ}{dt}. \tag{7}$$

In (6) and (7), Q and μ are the one-dimensional charge per unit length and the mobility, respectively. These are

the one-dimensional counterparts of the two-dimensional quantities discussed in Section II. The precise way in which the one-dimensional quantities are calculated will be discussed in Section III-B. V is the voltage along the one-dimensional model and I is the current flowing through it. The sign convention used makes both Q and μ negative. Substituting (6) into (7) gives

$$-\frac{dQ}{dt} = -Q\mu\frac{d^2V}{dx^2} - Q\frac{dV}{dx}\frac{d\mu}{dx} - \mu\frac{dV}{dx}\frac{dQ}{dx} + \gamma\left[\mu\frac{d^2Q}{dx^2} + \frac{dQ}{dx}\frac{d\mu}{dx}\right]. \quad (8)$$

We now consider Q, μ, and V to be the sum of a time-independent term and a time-dependent term using harmonic time variation:

$$Q = \bar{Q}_0 + \tilde{Q}e^{j\omega t} \quad (9)$$

$$V = \bar{V}_0 + \tilde{V}e^{j\omega t} \quad (10)$$

$$\mu = \bar{\mu}_0 + \tilde{\mu}e^{j\omega t}. \quad (11)$$

The bars over the steady-state values (those with "0" subscripts) are intended to distinguish them from their two-dimensional counterparts. Quantities with the tilde over them are the magnitudes of the time-varying components. The ac charge $\tilde{Q}$ is related to the ac voltage $\tilde{V}$ through the channel to gate capacitance C as described by the equation

$$\tilde{Q} = C\tilde{V}. \quad (12)$$

C will be determined later by reference to the results of the static solution.

The ac mobility can be found by expanding the mobility as a function of the total electric field in a Taylor series about the time average electric field:

$$\mu = f(\bar{E}_0 + \tilde{E}e^{j\omega t}) = f(\bar{E}_0) + \frac{\partial f}{\partial E}\bigg|_{E=\bar{E}_0}\tilde{E}e^{j\omega t} = \bar{\mu}_0 + \tilde{\mu}e^{j\omega t} \quad (13)$$

where $f(\bar{E})$ is the empirical expression due to Jaggi. Recognizing that $\tilde{\mu}e^{j\omega t}$ is equal to the second term in the expansion in (13) where f is given by (5), we obtain

$$\tilde{\mu} = \left[\frac{\partial v}{\partial E} - \bar{\mu}_0\right]\frac{\partial\tilde{V}}{\partial x}\left[\frac{\partial\bar{V}_0}{\partial x}\right]^{-1} \quad (14)$$

in which v is the total electron velocity and is equal to the product of the total electric field and the mobility as given in (5). Substituting (9) and (10) into (8) and keeping only the time-independent terms, (15) results:

$$\bar{Q}_0\bar{\mu}_0\frac{\partial^2\bar{V}_0}{\partial x^2} + \bar{Q}_0\frac{\partial\bar{V}_0}{\partial x}\frac{\partial\bar{\mu}_0}{\partial x} + \bar{\mu}_0\frac{\partial\bar{V}_0}{\partial x}\frac{\partial\bar{Q}_0}{\partial x} - \gamma\left[\bar{\mu}_0\frac{\partial^2\bar{Q}_0}{\partial x^2} + \frac{\partial\bar{Q}_0}{\partial x}\frac{\partial\bar{\mu}_0}{\partial x}\right] = 0. \quad (15)$$

Substituting (9)–(11) into (8) and keeping only the linear time-dependent terms, we have, using (12) for the relationship between ac charge and ac voltage and (14) for the ac mobility, the following equation in $\tilde{V}$:

$$\left[\bar{Q}_0\frac{\partial v}{\partial E} - \gamma\bar{\mu}_0 C - \gamma\frac{\partial\bar{Q}_0}{\partial x}\left(\frac{\partial v}{\partial E} - \bar{\mu}_0\right)\left(\frac{\partial\bar{V}_0}{\partial x}\right)^{-1}\right]\frac{\partial^2\tilde{V}}{\partial x^2} + \left[\bar{Q}_0\frac{\partial^2 v}{\partial E\partial x} + \bar{\mu}_0\frac{\partial\bar{V}_0}{\partial x}C + \frac{\partial v}{\partial E}\frac{\partial\bar{Q}_0}{\partial x} - 2\gamma\bar{\mu}_0\frac{\partial C}{\partial x} - \gamma\left(\frac{\partial v}{\partial E} - \bar{\mu}_0\right)\left(\frac{\partial\bar{V}_0}{\partial x}\right)^{-1}\frac{\partial^2\bar{Q}_0}{\partial x^2} + \gamma\frac{\partial\bar{Q}_0}{\partial x}\left(\frac{\partial v}{\partial E} - \bar{\mu}_0\right)\left(\frac{\partial\bar{V}_0}{\partial x}\right)^{-2}\frac{\partial^2\bar{V}_0}{\partial x^2} - \gamma\left(\frac{\partial^2 v}{\partial E\partial x} - \frac{\partial\bar{\mu}_0}{\partial x}\right)\left(\frac{\partial\bar{V}_0}{\partial x}\right)^{-1}\frac{\partial\bar{Q}_0}{\partial x} - \gamma\frac{\partial\bar{\mu}_0}{\partial x}C\right]\frac{\partial\tilde{V}}{\partial x} + \left[C\bar{\mu}_0\frac{\partial^2\bar{V}_0}{\partial x^2} + C\frac{\partial\bar{V}_0}{\partial x}\frac{\partial\bar{\mu}_0}{\partial x} + \bar{\mu}_0\frac{\partial\bar{V}_0}{\partial x}\frac{\partial C}{\partial x} - \gamma\bar{\mu}_0\frac{\partial^2 C}{\partial x^2} - \gamma\frac{\partial\bar{\mu}_0}{\partial x}\frac{\partial C}{\partial x} - j\omega C\right]\tilde{V} = 0. \quad (16)$$

The solutions to (16), subject to boundary conditions appropriate for y_{11} and y_{21}, or for y_{12} and y_{22}, give the ac voltage as a function of x in the one-dimensional model. In order to find the common gate y parameters, the ac current is also needed. By substituting (9)–(11) into (6) and keeping only the linear ac terms, an expression can be found relating the ac current to the ac voltage. Thus knowing $\tilde{V}$ from (16), $\tilde{I}$ can be found from (17):

$$\tilde{I} = -\bar{Q}_0\frac{\partial v}{\partial E}\frac{\partial\tilde{V}}{\partial x} - C\bar{\mu}_0\frac{\partial\bar{V}_0}{\partial x}\tilde{V} + \gamma\bar{\mu}_0 C\frac{\partial\tilde{V}}{\partial x} + \gamma\bar{\mu}_0\tilde{V}\frac{\partial C}{\partial x} + \gamma\left(\frac{\partial v}{\partial E} - \bar{\mu}_0\right)\left(\frac{\partial\bar{V}_0}{\partial x}\right)^{-1}\frac{\partial\bar{Q}_0}{\partial x}\frac{\partial\tilde{V}}{\partial x}. \quad (17)$$

The solution of (16) in conjunction with (17) gives the ac current and voltage from which a complete set of common gate short-circuit admittance parameters at a given frequency can be calculated. The common source y parameters can then be evaluated by way of a simple transformation.

B. Method of Evaluating Coefficients of (16)

In order to solve (16) the values of $\bar{Q}_0$, $\partial\bar{V}_0/\partial x$, $\bar{\mu}_0$, and C must be known as functions of x. The first three are the one-dimensional analogs of the two-dimensional values of charge, electric field, and mobility computed in the static case. The capacitance C will be found, as shown later in this section, using the difference of two static solutions. There is no way to uniquely calculate the first three quantities, so we have defined them in what appears to be

an intuitively reasonable way. This is described in the following paragraphs.

In the region between the source contact and the edge of the gate the current flow is rather uniform in the epitaxial layer. Thus the two-dimensional steady-state quantities Q_0, $\partial V_0/\partial x$, and μ_0 have nearly constant values there so that any averaging scheme will be satisfactory. Similar comments apply near the drain contact. It is only in the neighborhood of the gate that we must be careful since it is this region that is responsible for the active behavior of the device and since these parameters tend to vary rapidly in this region.

Since we are interested in the ac behavior of the device it seems most reasonable to be more concerned with those values of Q_0, $\partial V_0/\partial x$, and μ_0 in the region where the principal portion of the ac current flows. For this reason we have chosen to average $\partial V_0/\partial x$ and μ_0 in the y direction using the ac current as a weighting factor in order to find the one-dimensional analogs $\partial \bar{V}_0/\partial x$ and $\bar{\mu}_0$. ($\bar{Q}_0$ will be determined later using the continuity equation (15) and the known values of $\partial \bar{V}_0/\partial x$ and $\bar{\mu}_0$.) In equation form this implies

$$I_{aci} = \sum_{j=2}^{m-1} J_{acij} h_{yij} \tag{18}$$

$$\left.\frac{\partial \bar{V}_0}{ax}\right|_i = \frac{1}{I_{ac1}} \sum_{j=2}^{m-1} J_{acij} \left.\frac{\partial \bar{V}_0}{\partial x}\right|_{ij} h_{yij} \tag{19}$$

$$\bar{\mu}_0|_i = \frac{1}{I_{ac1}} \sum_{j=2}^{m-1} J_{acij} \bar{\mu}_{0ij} h_{yij}. \tag{20}$$

In (18)–(20) the subscript ij refers to column i (perpendicular to the gate) and row j (parallel to the gate) in the grid used to find the static solution. The summations are extended over the m rows of that same grid. h_{yij} is a grid spacing in the y direction at column j and row i. J_{acij} is the ac current density in the limit of zero frequency at column i and row j. J_{ac1j} is obtained by solving (1)–(5) twice with boundary conditions on the gate that differ by a few millivolts. By subtracting the current densities obtained from the two static solutions, the ac current densities are obtained as a function of x and y. Since the principal portion of the ac current is found to flow near the edge of the depletion region in the epitaxial layer, the use of J_{acij} as the weighting function results in average values that are most strongly influenced by that region of the device. The mobility μ_{0ij} is obtained by calculating the magnitude of the vector electric field at i, j and using (5) to find the mobility. In this way, we have included the effect of the y component of electric field on the x component of the electron velocity.

$\bar{Q}_0$ remains to be found. Having the one-dimensional $\bar{\mu}_0$ and $\partial \bar{V}_0/\partial x$ it is possible to calculate $\bar{Q}_0$. We know from (7) that at dc the channel current is continuous. Equation (15) can be interpreted as a second-order linear ordinary differential equation for $\bar{Q}_0$ involving $\bar{\mu}_0$ and $\partial \bar{V}_0/\partial x$. $\bar{\mu}_0$ and $\partial \bar{V}_0/\partial x$ are known from the two-dimensional solution by using the weighting functions given in (18)–(20). We also know that in the ohmic region, at the source and drain contacts, diffusion currents are not important. The charge per unit length $\bar{Q}_0$ at the source and drain contacts is then given by

$$\bar{Q}_0|_{\text{source}} = \left.\frac{I_{dc}}{\bar{\mu}_0(\partial \bar{V}_0/\partial x)}\right|_{\text{source}} \tag{21}$$

$$\bar{Q}_0|_{\text{drain}} = \left.\frac{I_{dc}}{\bar{\mu}_0(\partial \bar{V}_0/\partial x)}\right|_{\text{drain}}. \tag{22}$$

Equations (21) and (22) are then used as boundary conditions for (15). The solution of (15) gives the static charge per unit length in the one-dimensional model as a function of x. Plots of $\bar{\mu}_0$, $\partial \bar{V}_0/\partial x$, and $\bar{Q}_0$ are shown in Figs. 2, 3, and 4 and are for boundary conditions of $V_{DS} = 5.00$ V and $V_{GS} = 0$ V.

Equation (16) also involves the capacitance per unit length C between the channel and the gate. This is found by obtaining a static solution with a boundary condition of 0.0 V on the gate and a second static solution with a boundary condition of -0.060 V on the gate. In both cases the source has a potential of 0.0 V. By integrating the mobile charge densities over a given column for both solutions and subtracting the two values, the channel to gate capacitance at column i is found to be

$$C_i = \frac{Q_i|\,0 - Q_i|\,0.060}{0.060} \text{ F/m}. \tag{23}$$

In addition to the capacitance due to mobile charge in the channel we must add an additional term that gives the geometrical capacitance between the channel and ground. This is a parallel-plate capacitance determined using the substrate thickness as the plate spacing. In the region of the depletion layer the geometrical capacitance term is negligible, but in the region outside the depletion region it is the total capacitance. A plot of the total capacitance as a function of x is shown in Fig. 5 for $V_{DS} = 5.00$ V.

C. Substrate Effect

The method used to find $\bar{\mu}_0$ and $\partial \bar{V}_0/\partial x$ selects values corresponding to the active region in the epitaxial layer but does not include the effects of the substrate. As suggested by Reiser [4], the substrate acts as a resistor between source and drain.

This resistor is responsible for the large values of the common gate y_{22} and y_{12} when compared to a p-n junction FET with two gates and a line of symmetry parallel to the gate through the center of the channel. In order to include the substrate effects in our one-dimensional model, we have explicitly included an admittance between the source and drain of 2.5×10^{-3} mho. This value was obtained from two solutions of the static two-dimensional problem with slightly different boundary conditions on the drain.

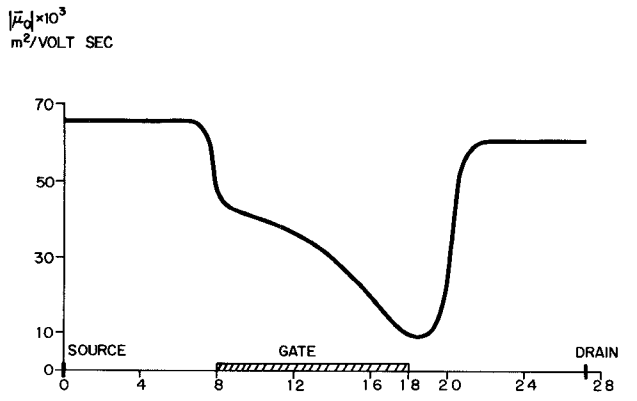

Fig. 2. Mobility as a function of x for the one-dimensional model with $V_{GS} = 0.0$ V and $V_{DS} = 5.0$ V.

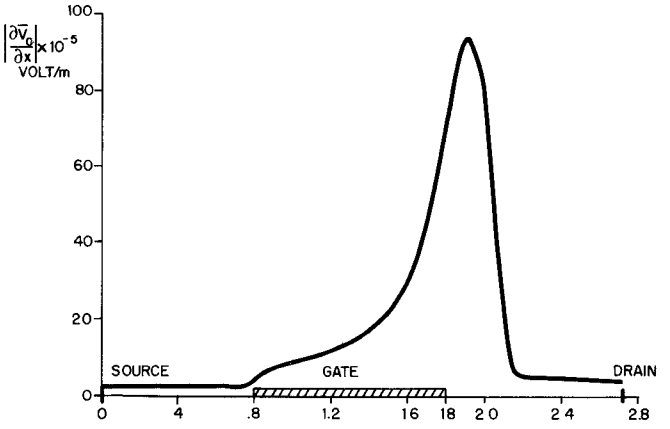

Fig. 3. Magnitude of the electric field as a function of x for the one-dimensional model with $V_{GS} = 0.0$ V and $V_{DS} = 5.0$ V.

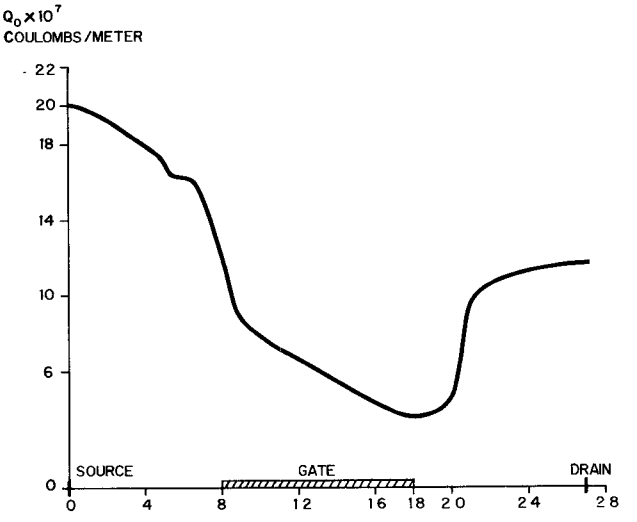

Fig. 4. Mobile charge density as a function of x for the one-dimensional model with $V_{GS} = 0.0$ V and $V_{DS} = 5.0$ V.

D. Numerical Method Used to Solve (15) and (16)

Both (15) and (16) are linear second-order ordinary differential equations with nonconstant coefficients subject to fixed boundary conditions at two points. Because

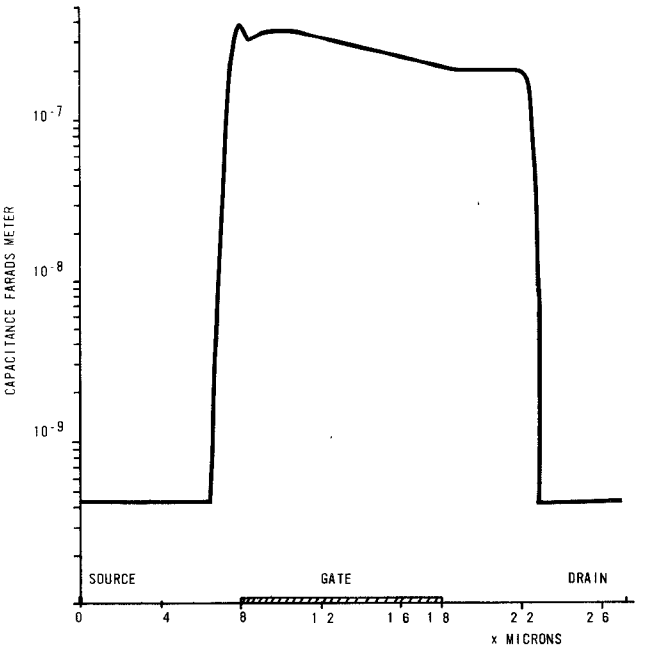

Fig. 5. Capacitance between the gate and channel as a function of x for the one-dimensional model with $V_{GS} = 0.0$ V and $V_{DS} = 5.0$ V.

we know the values of the coefficients of (15) and (16) only at discrete points and because of the complexity of these equations, solutions were found using numerical methods.

The derivatives in (15) and (16) are replaced by finite difference approximations accurate to order h^2 resulting in a set of linear equations of the form

$$C_p\alpha_w + A_p\alpha_p + B_p\alpha_E = 0, \qquad 2 \leq p \leq m \quad (24)$$

in which C_p, A_p, and B_p are constant, α_p is the desired variable value at a point, and α_E and α_W are its east and west neighbors, respectively. The set of equations (24) is a tridiagonal system, the solution to which may be found using an efficient algorithm given by Keller [12]. Given the two-dimensional static solutions, a Fortran IV program was written for an HW 635 machine that will solve for the y parameters at 110 frequencies in 0.1-h processor time. This requires the solution of (15) and 220 solutions of (16) with 110 values of the frequency and 2 sets of boundary conditions for each value of frequency.

Due to the large gradients of $\bar{\mu}_0$, $\partial \bar{V}_0/\partial x$, and C near the drain end of the gate as shown in Figs. 2, 3, and 5, a grid spacing smaller than that used in the static case was required in order to solve (16). The solution to (16) was checked at zero frequency by calculating the current at each grid point. Because no displacement currents flow at zero frequency, the current should be constant throughout the channel. In order to obtain current continuity, the grid spacing was reduced using a fourth-order Lagrange interpolation for points that do not coincide with the columns of the two-dimensional grid. In this fashion current continuity was achieved.

E. Results of the AC Solution

The common gate admittance parameters described in the analysis above were converted to common source y parameters and are shown as functions of frequency in Figs. 6–9 using $V_{GS} = 0.0$ V and $V_{DS} = 5.0$ V. The maximum available gain (MAG) [or the maximum stable gain (MSG)] and the stability factor computed from these parameters are shown in Fig. 10.

In order to evaluate the validity of the model that has been used, it is important to compare the calculated results with experimental measurements. The device whose properties we are trying to calculate (Fig. 1) has dimensions and impurity concentrations comparable with the device reported by Wolf [1].

A comparison of his results and our own is complicated by the presence of parasitic elements in the experimental device. The experimental device had two relatively large Schottky-barrier pads for the gate contacts that, in effect, add a resistor on the order of 400 Ω in parallel with the gate [1]. This has the effect of increasing the real part of y_{11} and reducing the MAG of the experimental device. Furthermore, as shown in Fig. 1, the theoretical model assumes that heavily doped regions, as could be

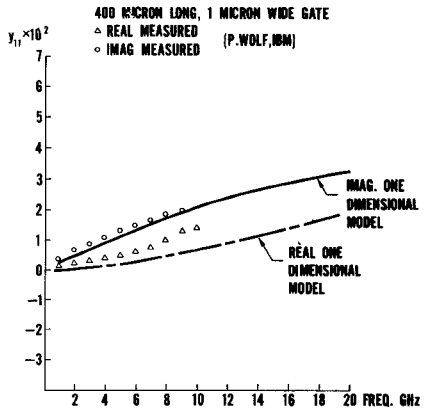

Fig. 6. y_{11S} in mhos as computed using the one-dimensional model with $V_{GS} = 0.0$ V and $V_{DS} = 5.0$ V and the experimental results of Wolf [1].

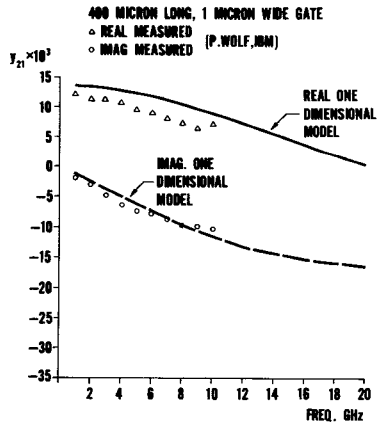

Fig. 7. y_{21S} in mhos as computed using the one-dimensional model with $V_{GS} = 0.0$ V and $V_{DS} = 5.0$ V and the experimental results of Wolf [1].

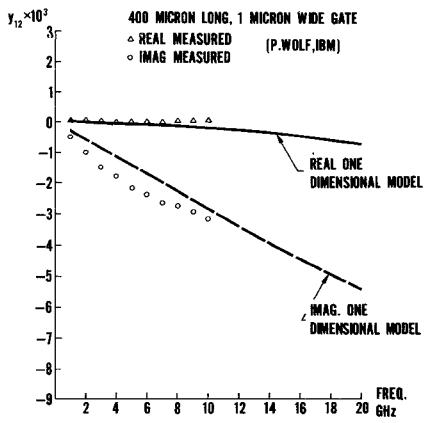

Fig. 8. y_{12S} in mhos as computed using the one-dimensional model with $V_{GS} = 0.0$ V and $V_{DS} = 5.0$ V and the experimental results of Wolf [1].

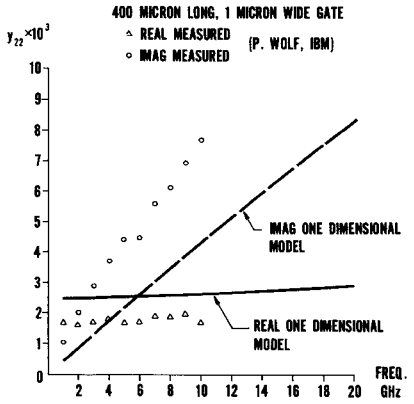

Fig. 9. y_{22S} in mhos as computed using the one-dimensional model with $V_{GS} = 0.0$ V and $V_{DS} = 5.0$ V and the experimental results of Wolf [1].

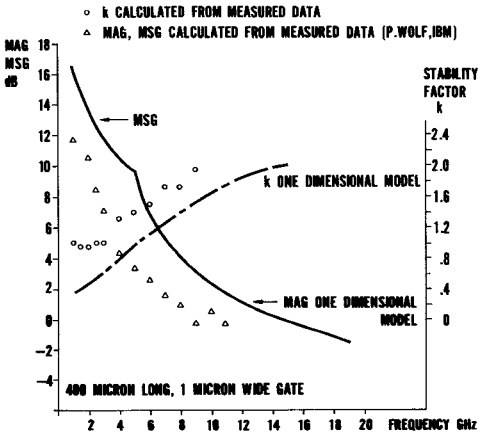

Fig. 10. Maximum stable gain (MSG), maximum available gain (MAG), and stability factor k as computed using the one-dimensional model with $V_{GS} = 0.0$ V, $V_{DS} = 5.0$ V, and the experimental results of Wolf [1].

obtained using ion implantation, exist under the source and drain contact metallizations to reduce the resistance in series with these contacts. The experimental device, however, had source and drain contacts directly on the epitaxial material. Finally, it is very difficult to measure accurately the physical dimensions and impurity con-

centrations and thus another uncertainty is introduced into the interpretation of the experimental data.

In order, therefore, to compare the experimental and theoretical results, we have tried to take these factors into account as well as we can. We have included in our calculated y parameters, shown in Figs. 6–10, both a resistance in series with the gate (R_G) equal to one-third of the gate metallization resistance and the geometrical capacitance between source and gate (C_{GS}) and between the gate and drain (C_{GD}) due to the contact metallizations [13]. The values used for these quantities are $R_G = 3.3\ \Omega$, $C_{GS} = 0.045$ pF, and $C_{GD} = 0.033$ pF. A detailed distributed analysis shows that these approximations are valid for frequency–gate length products of less than 2×10^6 Hz·m [8]. Since the experimental device reported by Wolf [1] has, in effect, four 100-μm-long gates in parallel, we are justified in making direct comparisons below 20 GHz.

It is apparent from Fig. 6 that the calculated value of the real part of y_{11} is slightly less than the experimental value. A large portion of this discrepancy is believed due to the gate pad parasitic in the experimental device. Figs. 7 and 8 show good agreement between calculated and measured values of y_{12} and y_{21}. The difference between calculated and measured values of the real part of y_{22} as shown in Fig. 9 is not nearly as significant as it appears due to the small magnitude of y_{22}. The error could be attributed to a deviation from a step junction at the substrate epitaxial layer boundary as assumed in our two-dimensional static model.

The MSG, the MAG, and the stability factor k are shown in Fig. 10 together with the experimental results of Wolf [1]. Calculated results show that the stability factor is less than 1 below 5 GHz so that the device is potentially unstable in this region. We have, therefore, shown the MSG in this region. The agreement between experiment and calculation is apparent. The maximum frequency of oscillation is reduced from 17.9 GHz to 14.7 GHz due to the parasitics associated with the 400-μm-long contact metallizations.

IV. Summary

The short-circuit admittance parameters of a Schottky-barrier field-effect transistor have been calculated and compared with the experimental characteristics of a similar device. Taking into account the parasitics in the experimental structure the agreement between experiment and theory is good. It is believed that the model developed to describe the high-frequency performance of the device will provide the device designer with the means to optimize this type of structure for use in microwave circuits.

Acknowledgment

The authors wish to thank Dr. K. A. Bishop for his guidance in the use of numerical methods, Dr. D. G. Daugherty for his comments during the course of this work, and G. L. Wright for his assistance in programming. The authors also wish to acknowledge the services provided by the Computation Center of the University of Kansas.

References

[1] P. Wolf, "Microwave properties of Schottky-barrier field effect transistors," *IBM J. Res. Develop.*, vol. 14, pp. 125–141, Mar. 1970.
[2] G. D. Alley and H. E. Talley, "A theoretical study of the high frequency performance of a Schottky barrier field effect transistor fabricated on a high resistivity substrate," presented at the IEEE Int. Electron Devices Meetings, Washington, D. C., Dec. 4–6, 1972.
[3] D. P. Kennedy and R. R. O'Brien, "Two dimensional analysis of J.F.E.T. structures containing a low conductivity substrate," *Electron. Lett.*, vol. 7, pp. 714–716, Dec. 2, 1971.
[4] M. Reiser, "Two dimensional analysis of substrate effects in junction FETS," *Electron. Lett.*, vol. 6, pp. 493–494, Aug. 6, 1970.
[5] R. Jaggi, "High-field electron drift velocities and current densities in silicon," *Helv. Phys. Acta*, vol. 42, Fasciculus Quartus, 1969.
[6] M. Reiser, "A two-dimensional numerical FET model for dc, ac, and large-signal analysis," *IEEE Trans. Electron Devices*, vol. ED-20, pp. 35–44, Jan. 1973.
[7] C.-K. Kim and E. S. Yang, "An analysis of current saturation mechanism of junction field-effect transistors," *IEEE Trans. Electron Devices*, vol. ED-17, pp. 120–127, Feb. 1970.
[8] G. D. Alley, H. E. Talley, and G. L. Wright, "Two-dimensional distributed theory for a microwave Schottky barrier field effect transistor," presented at the IEEE G-MTT Int. Microwave Symp., June 1973.
[9] K. E. Drangeid and R. Sommerhalder, "Dynamic performance of Schottky-barrier field effect transistors," *IBM J. Res. Develop.*, pp. 82–94, Mar. 1970.
[10] J. R. Hauser, "Small signal properties of field effect devices," *IEEE Trans. Electron Devices*, vol. ED-12, pp. 605–618, Dec. 1965.
[11] A. van der Ziel and J. W. Ero, "Small-signal, high-frequency theory of field-effect transistors," *IEEE Trans. Electron Devices*, vol. ED-11, pp. 28–135, Apr. 1964.
[12] H. B. Keller, *Numerical Methods for Two Point Boundary Value Problems*. Waltham, Mass.: Blaisdell, 1968.
[13] J. I. Smith, "The even- and odd-mode capacitance parameters for coupled lines in suspended substrated," *IEEE Trans. Microwave Theory Tech.*, vol. MTT-19, pp. 424–431, May 1971.